Climatic factors contributing to long-term variations of surface fine dust concentration in the United States

Bing Pu[1,2] and Paul Ginoux[2]

[1]Atmospheric and Oceanic Sciences Program, Princeton University,
Princeton, New Jersey 08544

[2]NOAA Geophysical Fluid Dynamics Laboratory, Princeton, New Jersey 08540

Correspondence to: Bing Pu (bpu@princeton.edu)

Abstract. High concentration of dust particles can cause respiratory problems and increase non-accidental mortality. Studies found fine dust (with aerodynamic diameter less than 2.5 microns) is an important component of the total PM2.5 mass in the western and central U.S. in spring and summer and has positive trends. This work examines climatic factors influencing long-term variations of surface fine dust concentration in the U.S. using station data from the Interagency Monitoring Protected Visual Environments (IMPROVE) network during 1990-2015. The variations of the fine dust concentration can be largely explained by the variations of precipitation, surface bareness, and 10 m wind speed. Moreover, including convective parameters such as convective inhibition (CIN) and convective available potential energy (CAPE) that reveal the stability of the atmosphere better explains the variations and trends over the Great Plains from spring to fall.

While the positive trend of fine dust concentration in the Southwest in spring is associated with precipitation deficit, the increase of fine dust over the central Great Plains in summer is largely associated with enhanced CIN and weakened CAPE, which are caused by increased atmospheric stability due to surface drying and lower troposphere warming. The strengthening of the Great Plains low-level jet also contributes to the increase of fine dust concentration in the central Great Plains in summer via its positive correlation with surface winds and negative correlation with CIN.

Summer dusty days in the central Great Plains are usually associated with a westward extension of the North Atlantic subtropical high that intensifies the Great Plains low-level jet and also results in a stable atmosphere with subsidence and reduced precipitation.

1. Introduction

Mineral dust is one of the most abundant atmospheric aerosols by mass. It is lifted to the atmosphere by strong wind from dry and bare surfaces. Severe dust storms have far-reaching socioeconomic impacts, affecting public transportation and health (e.g., Morman and Plumlee, 2013) by degrading visibility and causing traffic accidents, breathing problems, and lung disease. Dust storms are found to be associated with increases in non-accidental mortality in the U.S. during 1993-2005 (Crooks et al., 2016).

Major dust sources in the United States are located over the western and the central U.S. While several deserts are located over the western U.S., e.g., the Mojave, Sonoran, and northern Chihuahuan deserts, over the central U.S. the dust sources are largely anthropogenic, in association with agriculture activities (Ginoux et al., 2012). Climate models project a drying trend in the late half of the 21st century over the southwest and central U.S. (e.g., Seager et al., 2007; Cook et al., 2015), regions largely collocated with the major dust sources in the U.S. This raises questions such as how future dust activities will change in the U.S. To project future dust variations, we first need to understand how dust activity varies in the present day. Pu and Ginoux (2017) explored this question using dust optical depth (DOD) derived from MODIS Deep Blue (M-DB2) aerosol products during 2003-2015 and found that variations of dust activity in the U.S. are largely associated with precipitation, near surface wind speed, and surface bareness.

While DOD describes the total optical depth of dust aerosols with different sizes and is widely used to study climate-dust interactions, fine dust with aerodynamic diameter less than 2.5 μm is more frequently used for air quality purposes. Fine dust

contributes about 40-50% of total Particulate Matter 2.5 (PM2.5) mass over the southwestern U.S. in spring and about 20-30% over the southwestern to central U.S. in summer (Hand et al., 2017).

Stations in the network of the Interagency Monitoring of Protected Visual Environments (IMPROVE) have collected near surface PM2.5 samples in the U.S. since 1988 (Malm et al., 1994; Hand et al., 2011). Analysis of chemical elements is used to derive surface fine dust concentration. Due to its long temporal coverage, this dataset has been widely used to study long-term variations of surface fine dust in the U.S. Using IMPROVE data, Hand et al. (2016) found an increasing trend of fine dust in spring in the southwestern U.S. during 1995-2014 and related this trend to a negative Pacific decadal oscillation (PDO) from 2007 to 2014. Tong et al. (2017) also found a rapid increase of dust storm activity in the Southwest from 1988 to 2011 and related the trend to sea surface temperature variations in the Pacific. Later, Hand et al. (2017) examined the trends of IMPROVE fine dust concentration in different seasons from 2000 to 2014 and found positive trends over the southwestern U.S. in spring and over the central U.S. in summer and fall. Similarly, Zhang et al. (2017) also found a positive trend of fine dust over the central U.S. from 2005 to 2015 and suggested this trend may contribute to the increase of absorbing aerosol optical depth in the region. Nonetheless, the possible causes of the fine dust trends, especially the increase of fine dust over the central U.S., have not been thoroughly discussed by previous studies. Here, we explore the underlying factors driving the long-term variations of fine dust from 1990 to 2015. We start with local environmental factors and then examine the possible influence of the low-level jet over the Great Plains on fine dust concentration in summer.

93 The following section describes the data and analysis method used in the paper.
94 Section 3 presents our major results and conclusions are summarized in Section 4.
95
96 **2. Data and Methodology**
97 **2.1 IMPROVE fine dust**
98 IMPROVE stations are located in National Parks and wilderness areas in the
99 United States, with PM2.5 sampling performed twice weekly (Wednesday and Saturday;
100 Malm et al. 1994) prior to 2000 and every third day afterwards. Records from 204
101 stations within a domain of 15°-53°N and 60°-127°W are used in this study, and most of
102 the stations have data extending back more than 10 years (Fig. S1 in the Supplement).
103 Elemental concentration is determined from X-ray fluorescence, and fine dust
104 concentration is calculated using the concentrations of aluminum (Al), silicon (Si),
105 calcium (Ca), iron (Fe), and titanium (Ti) by assuming oxide norms associated with
106 predominant soil species (Malm et al., 1994; their Eq. 5). More details regarding
107 IMPROVE stations, sampling, and analysis method can be found in previous studies
108 (Hand et al., 2011; 2012; 2016; 2017).
109 We averaged daily station data to monthly means and then interpolated them to a
110 0.5° by 0.5° grid using inverse distance weighted interpolation, i.e., weights depending
111 on the inverse cubic distance between the site location and the interpolated grid point. All
112 daily data are used to calculate monthly mean. We tried the criteria of about 50%
113 completeness (i.e., at least 5 records in each month) for calculating monthly mean, and
114 the results are similar. In daily composite analysis, daily station data are interpolated to a
115 0.5° by 0.5° grid using the same method. Least squares linear trend analysis is applied to

116 the interpolated data, and student-t test is used for statistical significance test. We realize
117 that the time-varying station numbers could contribute to the uncertainties of our trend
118 analysis; so similar analysis is also applied to station data with long-term records (see
119 Fig. 1 for details).

120 Following Pu and Ginoux (2017), two dusty regions are selected for analysis. The
121 southwestern U.S. (WST for short; 32°-42°N, 105°-124°W) and Great Plains (GP for
122 short; 25°-49°N, 95°-105°W) cover the major dust source regions in the U.S. (black
123 boxes in Fig. 1). In later analysis, we also focused over the central Great Plains (CGP for
124 short; 32°-40°N, 95°-102°W) in summer to examine the positive trend of fine dust in the
125 region.

126

127 **2.2 Cloud-Aerosol Lidar with Orthogonal Polarization (CALIOP) products**

128 CALIOP is the two-wavelength polarization lidar carried by Cloud-Aerosol Lidar
129 and Infrared Pathfinder Satellite Observation (CALIPSO) satellite, which was launched
130 in April 2006 (Winker et al., 2004; 2007). CALIOP measures backscattered radiances
131 attenuated by the presence of aerosols and clouds, whose microphysical and optical
132 properties are retrieved. Daily products are available since June 2006. To examine the
133 vertical profile of dust concentration in the U.S., both the daily 532 nm total attenuated
134 backscatter from Level 1 product and the depolarization ratio from Level 2 product are
135 used. The depolarization ratio can be used to separate spherical and non-spherical
136 hydrometeors and aerosols (Sassen, 1991), and here a threshold of 0.2 is used to separate
137 non-spherical dust from other aerosols (Li et al., 2010).

138

2.2 Precipitation

The Precipitation Reconstruction over Land (PRECL; Chen et al., 2002) from the National Oceanic and Atmospheric Administration (NOAA) is a global analysis available monthly from 1948 to present at a 1° by 1° resolution. Its relative high-resolution and long records are suitable to study long-term connections between fine dust and precipitation. The dataset is derived from gauge observations from the Global Historical Climatology Network (GHCN), version 2, and the Climate Anomaly Monitoring System (CAMS) datasets. Monthly precipitation from 1990 to 2015 is used.

2.3 Leaf area index (LAI)

Monthly LAI derived from the version 4 of Climate Data Record (CDR) of Advanced Very High Resolution Radiometer (AVHRR) surface reflectance (Claverie et al., 2014) and produced by the National Aeronautics and Space Administration (NASA) Goddard Space Flight Center (GSFC) and the University of Maryland is used. The gridded monthly data are on a 0.05° by 0.05° horizontal resolution and available from 1981 to present. A detailed discussion on the algorithm and evaluation of the dataset can be found by Claverie et al. (2016). This dataset is selected due to its high spatial resolution and long temporal coverage. Monthly data from 1990 to 2015 are used.

Surface bareness is derived from seasonal mean LAI, and is calculated following Pu and Ginoux (2017),

$$Bareness = -exp(LAI) \quad . \tag{1}$$

2.4 Reanalysis

North American Regional Reanalysis (NARR; Mesinger et al., 2006) provides 3-hourly, daily, and monthly meteorological variables from 1979 to the present at a high spatial resolution (i.e., about 32km horizontally). Precipitation in the NARR is assimilated with observations. Here daily precipitation is used for daily composite analysis in section 3.3.2. The reanalysis reasonably captures the hydroclimatic fields in the continental U.S. on multiple time scales (Ruiz-Barradas and Nigam, 2006; Ruane, 2010a, b), thus is suitable to study the connection between fine dust concentration and local hydroclimatic variables. Daily and monthly convective variables such as convective inhibition (CIN), and convective available potential energy (CAPE) are used. CIN is defined as the energy that a parcel needs to overcome to rise above the level of free convection (LFC), and is usually written as:

$$CIN = -\int_{P_{sfc}}^{P_{LFC}} R_d\left(T_{vp} - T_{ve}\right) dlnp \quad , \tag{2}$$

where P_{LFC} is the pressure at LFC, P_{sfc} is the pressure at the surface, R_d is the specific gas constant for dry air, T_{vp} is the virtual temperature of the lifted parcel, and T_{ve} is the virtual temperature of the environment. CIN is usually a negative variable, with bigger CIN (in absolute value) indicating greater inhibition. On the other hand, CAPE describes the positive buoyancy of an air particle from the LFC to the equilibrium level (neutral buoyancy), and can be written as:

$$CAPE = -\int_{P_{LFC}}^{P_{EL}} R_d\left(T_{vp} - T_{ve}\right) dlnp \quad , \tag{3}$$

where P_{EL} is the pressure at the equilibrium level. Both CIN and CAPE describe the stability of the atmosphere, and usually convection easily occurs when CAPE is high and CIN is low (in absolute value; e.g., Colby, 1984; Riemann-Campe et al., 2009; Myoung

and Nielsen-Gammon, 2010a). Note the two variables can sometimes vary in opposite directions. Indeed, when CAPE is high, strong inhibition may still prohibit the occurrence of deep convection.

In addition, daily and monthly means of horizontal wind speed at 900 hPa, temperature at 700 hPa (T_{700}), 10 m wind speed, dew point temperature (T_{dp}), and 2 m air temperature (T_{2m}), total cloud cover, total and convective precipitation are used.

Another reanalysis used in this work is the ERA-Interim (Dee et al., 2011) from the European Centre for Medium-Range Weather Forecasts (ECMWF). ERA-Interim is a global reanalysis with a horizontal resolution of T255 (about 0.7° or 80 km) and 37 vertical levels, available from 1979 to present. It complements the regional reanalysis by providing a larger domain to analyze circulation variations and also a few surface variables (such as surface turbulent stress) that are not available in the NARR. 6-hourly analysis and 3-hourly forecast variables such as surface turbulent stress, vertical and horizontal winds, air temperature, and specific humidity from 1000 to 200 hPa, 850 hPa winds and geopotential height are used to calculate daily means of these variables.

2.5 Multiple-linear regression

To understand the connection between the potentially controlling factors and the variation of fine dust concentration, multiple-linear regressions are applied by regressing the observed gridded fine dust concentration onto 3, 4, or 5 standardized controlling factors, a method similar to the one used by Pu and Ginoux (2017). Since multiple controlling factors and gridded surface fine dust have different horizontal resolutions, for

207 the regression analysis we first interpolated all variables to a 1° by 1° grid, then apply
208 the regression at each grid point.

209 The fine dust concentration can be reconstructed by using the regression
210 coefficients and observed variations of the controlling factors (such as precipitation,
211 surface wind, and bareness). We focus our analysis on two statistical properties:
212 correlations of regional averaged time series and (centered) pattern correlations (e.g., Pu
213 et al., 2016b) for the trends. These two properties are calculated for both observed and
214 regression model estimated (i.e., reconstructed) fine dust concentrations.

215

216 **3. Results**

217 **3.1 Trends of surface fine dust concentration during 1990-2015 and local controlling**
218 **factors**

219 Figure 1 shows the trend of fine dust concentration from gridded data (shading)
220 and also those from stations with at least 23 years of consecutive records (colored circles)
221 from 1990 to 2015. Most long-term sites show trends similar to those from the
222 interpolated data, with a few exceptions, e.g., over northern Alabama, where interpolated
223 data show positive trends due to the influence of nearby stations with shorter records
224 (Fig. S1 in the Supplement). Significant positive trends are found over the southwestern
225 U.S. in spring (MAM), over the central to southern Great Plains in summer (JJA), and the
226 northern Great Plains in fall (SON). Dust concentration also increases over southwestern
227 Arizona (up to 0.06 μg m^{-3} yr^{-1}), by about 2.5% of its climatological value (Fig. S2 in the
228 Supplement) per year, in all seasons. A similar increasing trend of fine dust in southern
229 Arizona in spring from 1988 to 2009 is also noticed by Sorooshian et al. (2011). A

230 decreasing trend is found over the northeastern U.S. in all seasons as well. The overall
231 pattern is somewhat similar to the trend identified by Hand et al. (2017; their Fig. 9) for
232 2000-2014, who also found increasing trends of fine dust in the Southwest in spring and
233 over the CGP in summer. One thing we want to point out here is that most of the stations
234 in the Great Plains have records shorter than 15 years, with only three stations having
235 records for more than 25 years (Fig. S1 in the Supplement), therefore the positive trends
236 here are combinations of interpolated information from nearby stations in the early period
237 (before ~2002) and more reliable data largely from local stations in the late period.

238 As suggested by previous studies, the trend of fine dust may be biased due to
239 suspicious trends in some chemical species (Al, Si, and Ti) used to construct fine dust in
240 association with changes of analytical methods (e.g., Hyslop et al., 2015; Hand et al.,
241 2016; Hand et al., 2017). Fe has been suggested as a good proxy of fine dust since it's
242 more stable and is a key component of dust (Hand et al. 2016; 2017). We examined the
243 trend of fine Fe (Fig. S3 in the Supplement), and found the pattern is very similar to the
244 trend of fine dust. In fact, we found the correlations between seasonal mean fine dust and
245 Fe (both gridded data and long-term stations) are around 0.90 (significant at the 99%
246 confidence level) in most part of the U.S. during 1990-2015 (Fig. S4 in the Supplement).
247 This suggests the trends revealed directly from surface fine dust record are comparably
248 reliable as those calculated from Fe. So we use fine dust concentration for this analysis.

249 What are the dominant factors influencing the variations of surface fine dust
250 concentration? Hand et al. (2016) found that the PDO played an important role in the
251 variability of fine dust concentration over the Southwest in March by creating a windier,
252 drier, and less vegetated environment. We would like to extend their analysis to other

253 seasons and regions. In addition, we focus on identifying key controlling factors at the
254 local level because remote forcings such as the PDO influence dust variations through
255 their tele-connection with local controlling factors. Pu and Ginoux (2017) found that
256 local precipitation, surface bareness, and surface wind speed could explain 49% to 88%
257 of the variances of dust event frequency (derived from DOD) over the western U.S. and
258 the Great Plains in different seasons from 2003 to 2015. We first examine to what extent
259 these factors can explain the variance of near surface fine dust concentration. Similar to
260 Pu and Ginoux (2017), we do not separate the contribution from local emissions or
261 remote transport to the fine dust concentration, although contributions from Asian dust in
262 spring over the western U.S. (Fischer et al., 2009; Creamean et al., 2014; Yu et al., 2012)
263 and from North African dust in summer over the southeastern U.S. (Perry et al., 1997;
264 Prospero, 1999a) have been observed.

265 Figures 2a-d show the dominant controlling factor among precipitation, surface
266 wind, and bareness for fine dust concentration variations on the interannual time scale
267 from 1990-2015 at each grid point. Precipitation plays an important role in most parts of
268 the southern U.S. in winter. In spring, surface wind starts to dominate the variations of
269 fine dust along the Gulf coast and eastern Great Plains, consistent with the intensification
270 of the Great Plains low-level jet (e.g., Helfand and Schubert, 1995; Weaver and Nigam,
271 2008; Pu and Dickinson, 2014; Pu et al., 2016a) in April and May, while bareness is
272 important over the western Great Plains and the Midwest. During summer, the influence
273 of surface wind speed gets stronger, especially over western Arizona and the lower
274 Mississippi basin, whereas bareness and precipitation are also important in many parts of
275 the Great Plains and western U.S. Precipitation becomes the dominant factor over most

parts of the U.S. again in fall, with surface winds playing a weak role over the southeast and northeast coasts.

The regression coefficients obtained here share some similarity with those shown by Pu and Ginoux, (2017; their Fig 4) using DOD, e.g., the importance of surface bareness in the Great Plains in spring and summer. However, there are also quite large differences, likely due to different periods of regression and the fact that the DOD and surface fine dust concentration are not always linearly related to each other (Fig. S5 in the Supplement). Fine dust covers a small fraction of the total mass distribution of dust particles, thus the connections between fine dust concentration and the controlling factors could be different from those with the DOD. For example, the scavenging effect of precipitation is more efficient on small particles (e.g., Zender et al., 2003) and as a result precipitation generally plays an overall more important role on fine dust variations than on the DOD, especially in winter, spring, and fall.

The correlations of regional averaged time series between reconstructed fine dust concentration in the southwestern U.S. (using regression coefficients and observed variations of precipitation, surface wind, and bareness) and that from the IMPROVE range from 0.69 in fall to 0.82 in winter, indicating that the above three factors explain about 48% to 67% variances of fine dust in the Southwest from 1990 to 2015. Over the Great Plains, these factors only explain 32% to 48% variances statistically, much lower than over the Southwest. Also note the low confidence level of the regression coefficients over the CGP in summer (Fig. 2c), which indicates that the above three factors are not sufficient to well explain the variations of fine dust in the Great Plains.

298 The development of dust storms has long been related to convection and
299 atmospheric stability (e.g., Marsham et al., 2008; Cuesta et al., 2009). Here we examine
300 whether the variances of fine dust concentration and trend can be better represented by
301 adding CIN (i.e., four-factor) and both CIN and CAPE (i.e., five-factor) in addition to the
302 three factors (i.e., three-factor) discussed above.
303 Figure 2e shows correlations (blue bars) between the observed and the
304 reconstructed regional mean fine dust concentration using three-, four-, and five-factor
305 regressions, and corresponding pattern correlations (pink dots) between trends from the
306 observed and reconstructed fine dust for the Great Plains and the southwestern U.S. Over
307 the Great Plains, pattern correlations are largely improved when including CIN and
308 CAPE, especially in spring (from 0.30 to 0.89) and summer (from 0.34 to 0.93), although
309 slightly decrease in winter. The correlations of regional mean time series between the
310 reconstructed and observed fine dust are also slightly improved from three-factor
311 regression to five-factor regression. Over the Southwest, the improvement of pattern
312 correlation is smaller, and the correlations of time series change little when including
313 CIN and CAPE.
314 The collinearity among the factors used in the multiple linear regression can be
315 examined by the variance inflation factor (VIF; O'Brien, 2007; Abudu et al., 2011), and
316 usually values between 5 and 10 are considered high collinearity and the results of
317 regression are less reliable. Increasing the number of predictors in multiple linear
318 regression generally increase VIFs. The VIFs for three-factor regression are around 1 and
319 2 in most areas, with a few spots around 3 (not shown), while the VIFs for five-factor
320 regression are slightly higher, especially for CIN and CAPE over the Southwest (Figs. S6

and 7 in the Supplement). The increase of VIF and relatively weak improvement in the correlations in the Southwest when adding the convective factors suggest that three factors (precipitation, surface wind, and bareness) are sufficient to capture the variations and trend of surface fine dust in the region. Over the Great Plains, adding CIN and CAPE can better explain the variations.

We now examine key factors driving the observed positive trends of fine dust concentration in spring and summer, the dustiest seasons (Fig. S2 in the Supplement), based on the above analysis. Specifically, we focus on the positive trends of surface fine dust over the southwestern U.S. in spring and over the CGP in summer (Fig. 1b and c). Figure 3a shows the trend of observed and reconstructed fine dust concentrations in spring along with three components contributed to the reconstructed trend (i.e., from precipitation, bareness, and surface wind). The reconstructed trend (Reg (all)) largely captures the positive trend in the Southwest shown in the observation (Obs). Among the three factors, precipitation plays the most important role in contributing to the positive trend over the Southwest, consistent with its dominant role in explaining observed interannual variability (Fig. 2b). The increase of fine dust is mainly associated with a decreasing trend of precipitation in the Southwest (Fig. 3b). Such a drying trend has been related to an increase of anticyclonic conditions in the North East Pacific (Prein et al., 2016) and an intensification of Pacific trades during 2002-2012 (Delworth et al., 2015).

The reconstructed summer trend using coefficients from five-factor regression is very similar to the observation, with a pattern correlation of 0.95 in the domain (Fig. 4a). The positive trend over the CGP is largely contributed by CIN, with a positive center at northern Texas, western Kansas, and Oklahoma. Parts of the positive trend over

Oklahoma and western Kansas are contributed by CAPE. In fact, both CIN and CAPE have significant negative trends over the CGP, although the trend of CAPE is slightly weaker than that of CIN (Fig. 4b). A decrease of CIN (i.e., an increase in its absolute value) denotes an increasing inhibition of convection, while weakened CAPE denotes a decreasing instability associated with moist convection. Note that CIN is also significantly negatively correlated with fine dust concentration on interannual time scale (r= -0.39, p= 0.05). This again indicates that CIN plays a more important role than CAPE in the recent positive trend of fine dust.

Both the trends of the CIN and CAPE denote an increase of atmospheric stability. Changes of CIN and CAPE have been related to boundary layer or near-surface temperature and moisture (e.g., Ye et al., 1998; Gettelman et al., 2002; Alappattu and Kunhikrishnan, 2009). Myoung and Nielsen-Gammon (2010b) found that the variations of CIN over Texas in the warm season can be well represented by the differences of temperature at 700 hPa (T_{700}) and surface dew point temperature (T_{dp}), i.e., T_{700}-T_{dp}. While T_{700} is a good proxy for temperature at the free-troposphere below the LFC, T_{dp} denotes the dryness at the surface. Thus, T_{700}-T_{dp} represents a joint effect of surface drying and warming at 700 hPa, a positive anomaly of which indicates increased atmospheric stability. Here we find both CIN and CAPE have significant negative correlations with T_{700}-T_{dp} over the CGP (Fig. 4c). A significant positive trend of T_{700}-T_{dp} is also found, supporting the assumption that the atmospheric stability is enhanced during the period. Such a changes of stability is largely due to the increase of T_{700}, although surface drying also contributes.

CIN is also found to be significantly correlated with rain days (daily precipitation $\geq$ 1 mm day^{-1}) in summer in Texas (Myoung and Nielsen-Gammon, 2010b). Here a similar positive correlation between CIN and rain days in the CGP is also found from 1990 to 2015 ($r=0.79$, $p<0.001$), suggesting that CIN could influence fine dust concentration via its connection with rain days. A stable atmosphere prevents deep moist convection, which reduces the chance of scavenging by precipitation, and also likely prevents dilution of fine dust concentration in the boundary layer with the clean air above through convective mixing. The connection underlying CIN and fine dust concentration is further discussed in section 3.3 using daily data.

3.2 The connection between the Great Plains low-level jet and summertime fine dust variations in the CGP

An important feature related to the moisture and heat transport and precipitation in the Great Plains from late spring to summer is the Great Plains low-level jet, which develops in April and reaches its maximum wind speed in June and July at around 900 hPa (e.g., Weaver and Nigam, 2008; Pu et al., 2016a). The southerly jet covers most of the southern to CGP, and turns into a westerly around 40° N passing through the Midwest. How this jet may influence the dust concentration in the CGP in summer is examined here.

Figure 5a shows the time series of the jet index in summer following the definition of Weaver and Nigam (2008) by averaging 900 hPa meridional wind speed at the jet core (25°-35°N, 97°-102°W) from 1990 to 2015. The jet index is significantly positively correlated with fine dust concentration in the CGP in summer ($r= 0.56$, $p<0.01$)

389 and also has a significant positive trend, suggesting that the jet also contributes to the
390 increasing of fine dust in the CGP. Such a positive connection between the jet and fine
391 dust concentration can be explained by jet's negative correlation with CIN and positive
392 correlation with the near surface wind speed in the CGP (Figs. 5b). An intensified jet
393 increases the near surface wind speed and meanwhile increases the stability of
394 atmosphere over the CGP by advecting moisture away to the Midwest.

395 Because most of the IMPROVE sites (4 out of 6) in the CGP only have records
396 since 2002, correlations between the jet index and fine dust concentration, CIN, and
397 surface wind for 2002-2015 are also calculated (Fig. 5c). The patterns are similar to those
398 during 1990-2015.

399 Dust from Africa can be transported to the southeastern U.S. and even Texas in
400 summer (e.g., Perry et al., 1997; Prospero, 1999b, a; 2010; 2014; Bozlaker et al., 2013).
401 Can the intensified jet transport more African dust and thus contribute to the increase of
402 fine dust in the CGP? Fully addressing this question will require a dust model that can
403 well reproduce the emission and transport processes of African dust, which is beyond the
404 scope of this paper. Here we discuss this question based on observational analysis. The
405 regression and trend analysis above suggests that local atmospheric stability largely
406 contributes to the positive trend. Since African dust is transported to the continental U.S.
407 passing through the Caribbean Sea and the Gulf of Mexico, we assume that the variations
408 of fine dust in stations nearby would reveal the influence of African dust. Two of such
409 stations, VIIS1 (18.3°N, 64.8°W) in the Virgin Islands National Park and EVER1
410 (25.4°N, 80.7°W) in the Everglades National Park, are used. It is found that the records
411 from these stations have significantly positive correlations with fine dust concentration

412 over the southeastern U.S. in JJA, but not over the CGP (Fig. S8 in the Supplement). This
413 suggests that the influence of African dust is largely over the Southeast on seasonal
414 mean, consistent with the results of Hand et al. (2017), who found the influence of North
415 African dust are mainly over the Southeast, Appalachia, and Virgin islands regions in
416 summer as indicated by a shift of elemental composition in IMPROVE sites.
417
418 **3.3 Factors contributing to high dust concentration over the CGP in summer**
419 While the negative correlation between fine dust concentration and precipitation
420 in the Southwest is straightforward, the correlation between fine dust and CIN in the CGP
421 is less obvious. Here we further examine the connection between fine dust and CIN and
422 other factors associated with high dust concentration in the area using daily events. As
423 mentioned earlier, since most stations in the CGP have records since 2002, the following
424 analysis focuses on summer during 2002-2015.
425
426 **3.3.1 Connection between surface fine dust concentration and CIN**
427 What's the physical connection between CIN and surface fine dust concentration?
428 Here we first explore the connection between CIN and a variable that is closely related to
429 dust emission. Figures 6a-c show the scatter plot of standardized (means are removed and
430 then divided by one standard deviation) CIN and friction velocity (U^*) anomalies, for all
431 the days in summer from 2002 to 2015, days when IMPROVE records are available (431
432 days), and dusty days, defined as days when daily anomaly of IMPROVE observation is
433 greater than one standard deviation (52 days), respectively. U^* is defined as the
434 following,

$$U^* = ([\tau/\rho])^{1/2} = [(\overline{u'w'})^2 + (\overline{v'w'})^2]^{1/4} \quad , \qquad (4)$$

where τ is the Reynolds stress and ρ is air density, and $\overline{u'w'}$ and $\overline{v'w'}$ are vertical flux of horizontal momentum. We calculated U^* using components of surface turbulent stress ($-\rho\overline{u'w'}$, $-\rho\overline{v'w'}$) from the ERA-Interim. U^* has long been related to dust emission (e.g., Gillette and Passi, 1988; Marticorena and Bergametti, 1995; Zender et al., 2003). As shown in Figs. 6a-c, CIN is significantly negatively related to U^* in all summer days and dusty days. This indicates a large negative CIN, or great inhibition for convection, is related to stronger near surface turbulent fluxes and U^*. How does CIN influence U^*?

In the CGP, both CIN and U^* are significantly correlated with near surface temperature, T_{2m}, in JJA and for days when fine dust records are available (Table 1), indicating that CIN is connected with U^* via their mutual connection with near surface temperature. Note such a connection seems not valid during dusty days (correlation between T_{2m} and U^* is not significant). Similarly, we found significant correlations between CIN and T_{700}-T_{dp}, and between T_{700}-T_{dp} and U^* (Table 1). This again, suggests that CIN is connected with U^* via its connection with surface variables such as temperature and dryness. Variables in Table 1 are all from the ERA-Interim (except CIN) to be consistent with U^*, results are similar if using NARR variables.

One hypothesis for the connection between CIN and U^* in dusty days is shown in Table 2. A significant positive correlation between CIN and vertical wind at 850 hPa (w850) is found, indicating that when the inhibition is strong, it favors subsidence. This is consistent with the finding by Riemann-Campe et al. (2009) who found in climatology high CIN value is located over subtropical regions with strong subsidence. The subsidence may transport momentum downward and promote U^*. This is consistent with

458 the negative correlation between U^* and w850 (Table 2). However, we also notice that
459 the above connections in dusty days are not valid if using w850 from the NARR,
460 suggesting further investigation on this mechanism is needed.

461 In addition to the connection between CIN and surface variables, the possible
462 mechanism that strong inhibition prevents dilution is also examined. We found four
463 examples in CALIOP snapshots over the CGP when the daily anomaly of near surface
464 fine dust concentration from the IMPROVE network is greater than one standard
465 deviation. Figure 7 shows nighttime 532 nm total attenuated backscatter (shading) on
466 August 10th, 2007 (top) and on June 21st, 2013 (bottom). Black contours show area with
467 depolarization ratio $\geq$ 0.2, denoting dust aerosols. In both cases, the inhibition is quite
468 strong, with daily CIN anomaly greater than one standard deviation. The difference
469 between the two cases is that on June 21st, 2013, CAPE is higher, which leads to some
470 convection as denoted by the clouds above. However, in both cases, with strong
471 inhibition, dust particles are largely located in a layer between the surface and 2 km.
472 Figure 8 shows a different situation when CIN has positive anomaly (i.e., weak
473 inhibition). In these cases, dust particle extends up to 4 km, and surface fine dust
474 concentrations in the CGP (with anomalies of 2.3 and 2.1 μg m^{-3}) are also lower than
475 those in Fig. 7 (with anomalies of 4.0 and 7.1 μg m^{-3}). Nonetheless, more cases are
476 needed to further verify this mechanism. The anomalous high fine dust concentration in
477 Everglades National Park (Figs. 7-8) in three of the four cases shown here suggest that
478 there may be a contribution from African dust in these days, but further analysis are
479 needed to clarify the magnitude of its contribution.
480

481 **3.3.2 Large-scale circulation pattern in dusty days**

482 Figure 9 shows the daily composites of related meteorological variables in dusty
483 days, i.e., when daily anomaly of CGP fine dust concentration is greater than one
484 standard deviation. Anomalous high fine dust concentration is associated with a reduced
485 CIN (Fig. 9b) in the CGP, but not so much with CAPE (Fig. 9c). CAPE is anomalously
486 enhanced over the northern Plains and the Midwest. Both the Great Plains low-level jet,
487 near surface wind, and friction velocity are enhanced (Figs. 9d-f). Precipitation (mostly
488 convective precipitation) in the CGP also decreases with reduced cloud cover, but
489 increases in the north (Figs. 9g-i), consistent with enhanced CAPE there. These features
490 are quite consistent with our analysis above on the favorable condition of enhanced fine
491 dust in the CGP.

492 Figure 10 shows the composites of vertical velocity (shading), vertical and
493 meridional wind vectors, specific humidity (purple contours), and potential temperature
494 (grey contours) zonally averaged over the CGP (95° -102° W), along with fine dust
495 concentration (orange line). Anomalous dry subsidence is centered at 30°-36°N, with
496 anomalous southerly winds at low-level associated with an intensified jet, while a rising
497 motion of moist air is located around 38-42°N with a maximum at 700-400 hPa. The
498 dipole pattern of anomalous vertical velocity is consistent with the precipitation anomaly
499 in the area (Figs. 9g-h). The anomalous potential temperature contour is quite uniform
500 near the surface at 30°-36°N with an inversion around 700 hPa, indicating a well-mixed
501 boundary layer in the region with increased fine dust.

502 What causes the changes of atmospheric stability, precipitation, and winds?
503 Figure 11 shows the composites of T_{2m} and geopotential height and winds at 850 hPa

504 during dusty days. Following Li et al. (2012a), 1560 gpm contour is used here to denote
505 the western edge of the North Atlantic subtropical high in the 2002-2015 climatology
506 (blue) and in dusty days (red). A westward extension of the subtropical high during dust
507 days is quite evident, with enhanced geopotential height over the southeastern U.S. and
508 the Gulf of Mexico (Fig. 11b). Such a westward extension of the subtropical high
509 intensifies the low-level jet by increasing the zonal pressure gradient, and also contributes
510 to the anomalous precipitation and vertical velocity patterns, as similar patterns are found
511 in previous studies associated with a westward extension of the subtropical high (e.g., Li
512 et al., 2012a; their Figs. 3a and 4a). The formation of the North Atlantic subtropical high
513 has been related to the land-sea heating contrast (Wu and Liu, 2003; Liu et al., 2004;
514 Miyasaka and Nakamura, 2005; Li et al., 2012a; Li et al., 2012b). One possible reason of
515 the westward extension of the subtropical high is the anomalous surface warming over
516 large part of the central and eastern U.S. (Fig. 11a) in dusty days that enhances the land-
517 sea temperature gradient.
518
519 **4. Conclusions**
520 Fine dust is an important component in the total PM 2.5 mass in the western to
521 central U.S. in spring and summer (Hand et al. 2017). Previous studies found positive
522 trends of fine dust concentration in the southwestern U.S. in spring and the central U.S. in
523 summer in the past 20 years (Hand et al., 2016; 2017; Zhang et al., 2017), but the
524 underlying causes are not clear, especially for the positive trend over the central U.S.
525 This study examined local controlling factors associated with variations of near surface
526 fine dust concentration from Interagency Monitoring of Protected Visual Environments

527 (IMPROVE) stations for 1990-2015. While precipitation, surface bareness, and surface
528 wind speed largely control the variation of fine dust concentration in the southwestern
529 U.S., including two convective parameters that reveal the stability of the atmosphere,
530 convective inhibition (CIN) and convective available potential energy (CAPE), better
531 explains the variations over the Great Plains from spring to fall.

532 In particular, we found that the increasing trend of fine dust concentration over
533 the Southwest in spring is associated with a significantly decreasing trend of
534 precipitation, while the positive trend of fine dust over the central Great Plains (CGP) is
535 largely due to enhanced atmospheric stability revealed by enhanced CIN (greater
536 inhibition) and decreased CAPE. Such a stability change is associated with surface drying
537 and warming in the lower troposphere around 700 hPa, i.e., a positive trend of T_{700}-T_{dp}. A
538 stable atmosphere prevents moist convection that can remove fine dust by in-cloud or
539 precipitation scavenging and also likely prevents the dilution of fine dust concentration
540 by prohibiting convective mixing between the dusty boundary layer air and the clean air
541 above.

542 The variations of the fine dust concentration in the CGP are also significantly
543 correlated to the Great Plains low-level jet, with a stronger jet corresponding to higher
544 fine dust concentration. Such a connection is largely due to jet's positive correlation with
545 surface wind speed and negative correlation with CIN.

546 The influence of CIN on dust emission in the CGP is examined using daily data in
547 summer. It is found that CIN is significantly negatively related to surface friction velocity
548 (U^*), i.e., with greater inhibition in association with stronger U^*. Such a connection is
549 largely due to CIN's connection with surface variables such as 2m temperature and dew

point temperature. During dusty days, another possible connection is that the anomalous subsidence associated with strong inhibition may transport momentum downward and increase surface U^*.

Dusty days in the CGP in summer are associated with a westward extension of the North Atlantic subtropical high that intensifies the Great Plains low-level jet and surface wind speed, increases atmospheric stability, and also creates anomalous subsidence over the southern to central Great Plains and reduces precipitation. The westward extension of the subtropical high is likely associated with the anomalous surface warming over the central to eastern U.S.

Our findings have important implications for future projections of fine dust variation in the U.S. Climate models have projected drying trends over the southwestern and the central U.S. (e.g., Seager et al., 2007; Cook et al., 2015) as well as an intensification of the North Atlantic subtropical high (Li et al., 2012b) in the late 21st century, all favorable to an increase of fine dust in the Southwest and CGP. Whether current increasing trends of fine dust will persist into the future requires further investigations that include factors not discussed here such as changes of anthropogenic land use, local synoptic-scale systems (e.g., cyclones and fronts), and remote forcings.

Acknowledgements.

IMPROVE is a collaborative association of state, tribal, and federal agencies, and international partners. US Environmental Protection Agency is the primary funding source, with contracting and research support from the National Park Service. The Air Quality Group at the University of California, Davis is the central analytical laboratory, with ion analysis provided by Research Triangle Institute, and carbon analysis provided by Desert Research Institute. IMPROVE fine dust data is downloaded from http://views.cira.colostate.edu/fed/DataWizard/. AVHRR leaf area index data are available at: ftp://eclipse.ncdc.noaa.gov/pub/cdr/lai-fapar/files/. PRECL Precipitation data are provided by the NOAA/OAR/ESRL PSD, Boulder, Colorado, USA, from their web site at http://www.esrl.noaa.gov/psd/. The CALIPSO products are downloaded from https://www-calipso.larc.nasa.gov/tools/data_avail/dpo_read.php?y=2007&m=08&d=10. The NCEP/NCAR reanalysis product is obtained from http://www.esrl.noaa.gov/psd/data/gridded/data.ncep.reanalysis.html and the ERA-Interim is downloaded from http://www.ecmwf.int/en/research/climate-reanalysis/era-interim. The NARR reanalysis is downloaded from https://www.esrl.noaa.gov/psd/data/gridded/data.narr.html. This research is supported by NOAA and Princeton University's Cooperative Institute for Climate Science and NASA under grant NNH14ZDA001N-ACMAP. The authors thank Drs. Stuart Evans and Jordan Schnell for their helpful comments on the early version of this paper. The insightful comments from Professor Patrick Chuang and the other reviewer help improved the paper and are sincerely appreciated.

596 References

597 Abudu, S., Cui, C. L., King, J. P., Moreno, J., and Bawazir, A. S.: Modeling of daily pan
598 evaporation using partial least squares regression, Sci China Technol Sc, 54, 163-
599 174, 10.1007/s11431-010-4205-z, 2011.
600 Alappattu, D. P., and Kunhikrishnan, P. K.: Premonsoon estimates of convective
601 available potential energy over the oceanic region surrounding the Indian
602 subcontinent, J Geophys Res-Atmos, 114, 10.1029/2008jd011521, 2009.
603 Bozlaker, A., Prospero, J. M., Fraser, M. P., and Chellam, S.: Quantifying the
604 Contribution of Long-Range Saharan Dust Transport on Particulate Matter
605 Concentrations in Houston, Texas, Using Detailed Elemental Analysis, Environ
606 Sci Technol, 47, 10179-10187, 10.1021/es4015663, 2013.
607 Chen, M. Y., Xie, P. P., Janowiak, J. E., and Arkin, P. A.: Global land precipitation: A
608 50-yr monthly analysis based on gauge observations, J Hydrometeorol, 3, 249-
609 266, Doi 10.1175/1525-7541(2002)003<0249:Glpaym>2.0.Co;2, 2002.
610 Claverie, M., Vermote, E., and NOAA-CDR-Program: NOAA Climate Data Record
611 (CDR) of Leaf Area Index (LAI) and Fraction of Absorbed Photosynthetically
612 Active Radiation (FAPAR), Version 4, NOAA National Climatic Data Center,
613 10.7289/V5M043BX, 2014.
614 Claverie, M., Matthews, J. L., Vermote, E. F., and Justice, C. O.: A 30+ Year AVHRR
615 LAI and FAPAR Climate Data Record: Algorithm Description and Validation,
616 Remote Sens-Basel, 8, 10.3390/rs8030263, 2016.

617 Colby, F. P.: Convective Inhibition as a Predictor of Convection during Ave-Sesame-Ii,
618 Mon Weather Rev, 112, 2239-2252, Doi 10.1175/1520-
619 0493(1984)112<2239:Ciaapo>2.0.Co;2, 1984.
620 Cook, B. I., Ault, T. R., and Smerdon, J. E.: Unprecedented 21st century drought risk in
621 the American Southwest and Central Plains, Science Advances, 1, 1-7,
622 10.1126/sciadv.1400082 2015.
623 Creamean, J. M., Spackman, J. R., Davis, S. M., and White, A. B.: Climatology of long-
624 range transported Asian dust along the West Coast of the United States, J
625 Geophys Res-Atmos, 119, 12171-12185, 10.1002/2014jd021694, 2014.
626 Crooks, J. L., Cascio, W. E., Percy, M. S., Reyes, J., Neas, L. M., and Hilborn, E. D.: The
627 Association between Dust Storms and Daily Non-Accidental Mortality in the
628 United States, 1993-2005, Environ Health Persp, 124, 1735-1743,
629 10.1289/Ehp216, 2016.
630 Cuesta, J., Marsham, J. H., Parker, D. J., and Flamant, C.: Dynamical mechanisms
631 controlling the vertical redistribution of dust and the thermodynamic structure of
632 the West Saharan atmospheric boundary layer during summer, Atmos Sci Lett,
633 10, 34-42, 10.1002/asl.207, 2009.
634 Dee, D. P., Uppala, S. M., Simmons, A. J., Berrisford, P., Poli, P., Kobayashi, S., Andrae,
635 U., Balmaseda, M. A., Balsamo, G., Bauer, P., Bechtold, P., Beljaars, A. C. M.,
636 van de Berg, L., Bidlot, J., Bormann, N., Delsol, C., Dragani, R., Fuentes, M.,
637 Geer, A. J., Haimberger, L., Healy, S. B., Hersbach, H., Holm, E. V., Isaksen, L.,
638 Kallberg, P., Kohler, M., Matricardi, M., McNally, A. P., Monge-Sanz, B. M.,
639 Morcrette, J. J., Park, B. K., Peubey, C., de Rosnay, P., Tavolato, C., Thepaut, J.

N., and Vitart, F.: The ERA-Interim reanalysis: configuration and performance of the data assimilation system, Q J Roy Meteor Soc, 137, 553-597, 10.1002/qj.828, 2011.

Delworth, T. L., Zeng, F. R., Rosati, A., Vecchi, G. A., and Wittenberg, A. T.: A Link between the Hiatus in Global Warming and North American Drought, J Climate, 28, 3834-3845, 10.1175/Jcli-D-14-00616.1, 2015.

Fischer, E. V., Hsu, N. C., Jaffe, D. A., Jeong, M. J., and Gong, S. L.: A decade of dust: Asian dust and springtime aerosol load in the US Pacific Northwest, Geophys Res Lett, 36, 10.1029/2008gl036467, 2009.

Gettelman, A., Seidel, D. J., Wheeler, M. C., and Ross, R. J.: Multidecadal trends in tropical convective available potential energy, J Geophys Res-Atmos, 107, 10.1029/2001jd001082, 2002.

Gillette, D. A., and Passi, R.: Modeling Dust Emission Caused by Wind Erosion, J Geophys Res-Atmos, 93, 14233-14242, DOI 10.1029/JD093iD11p14233, 1988.

Ginoux, P., Prospero, J. M., Gill, T. E., Hsu, N. C., and Zhao, M.: Global-Scale Attribution of Anthropogenic and Natural Dust Sources and Their Emission Rates Based on Modis Deep Blue Aerosol Products, Rev Geophys, 50, 10.1029/2012rg000388, 2012.

Hand, J. L., Copeland, S. A., Day, D. E., Dillner, A. M., Indresand, H., Malm, W. C., McDade, C. E., Moore, C. T., Pitchford, M. L., Schichtel, B. A., and Watson, J. G.: IMPROVE (Interagency Monitoring of Protected Visual Environments): Spatial and seasonal patterns and temporal variability of haze and its constituents in the United States, 2011.

663 Hand, J. L., Schichtel, B. A., Pitchford, M., Malm, W. C., and Frank, N. H.: Seasonal
664 composition of remote and urban fine particulate matter in the United States, J
665 Geophys Res-Atmos, 117, 10.1029/2011jd017122, 2012.
666 Hand, J. L., White, W. H., Gebhart, K. A., Hyslop, N. P., Gill, T. E., and Schichtel, B. A.:
667 Earlier onset of the spring fine dust season in the southwestern United States,
668 Geophys Res Lett, 43, 4001-4009, 10.1002/2016gl068519, 2016.
669 Hand, J. L., Gill, T. E., and Schichtel, B. A.: Spatial and seasonal variability in fine
670 mineral dust and coarse aerosol mass at remote sites across the United States, J
671 Geophys Res-Atmos, 122, 3080-3097, 10.1002/2016jd026290, 2017.
672 Helfand, H. M., and Schubert, S. D.: Climatology of the Simulated Great-Plains Low-
673 Level Jet and Its Contribution to the Continental Moisture Budget of the United-
674 States, J Climate, 8, 784-806, Doi 10.1175/1520-
675 0442(1995)008<0784:Cotsgp>2.0.Co;2, 1995.
676 Hyslop, N. P., Trzepla, K., and White, W. H.: Assessing the Suitability of Historical
677 PM2.5 Element Measurements for Trend Analysis, Environ Sci Technol, 49,
678 9247-9255, 10.1021/acs.est.5b01572, 2015.
679 Li, F. Y., Ginoux, P., and Ramaswamy, V.: Transport of Patagonian dust to Antarctica, J
680 Geophys Res-Atmos, 115, 10.1029/2009jd012356, 2010.
681 Li, L. F., Li, W. H., and Kushnir, Y.: Variation of the North Atlantic subtropical high
682 western ridge and its implication to Southeastern US summer precipitation, Clim
683 Dynam, 39, 1401-1412, 10.1007/s00382-011-1214-y, 2012a.

684 Li, W. H., Li, L. F., Ting, M. F., and Liu, Y. M.: Intensification of Northern Hemisphere
685 subtropical highs in a warming climate, Nat Geosci, 5, 830-834,
686 10.1038/Ngeo1590, 2012b.
687 Liu, Y. M., Wu, G. X., and Ren, R. C.: Relationship between the subtropical anticyclone
688 and diabatic heating, J Climate, 17, 682-698, Doi 10.1175/1520-
689 0442(2004)017<0682:Rbtsaa>2.0.Co;2, 2004.
690 Malm, W. C., Sisler, J. F., Huffman, D., Eldred, R. A., and Cahill, T. A.: Spatial and
691 Seasonal Trends in Particle Concentration and Optical Extinction in the United-
692 States, J Geophys Res-Atmos, 99, 1347-1370, Doi 10.1029/93jd02916, 1994.
693 Marsham, J. H., Parker, D. J., Grams, C. M., Taylor, C. M., and Haywood, J. M.: Uplift
694 of Saharan dust south of the intertropical discontinuity, J Geophys Res-Atmos,
695 113, 10.1029/2008jd009844, 2008.
696 Marticorena, B., and Bergametti, G.: Modeling the Atmospheric Dust Cycle .1. Design of
697 a Soil-Derived Dust Emission Scheme, J Geophys Res-Atmos, 100, 16415-16430,
698 Doi 10.1029/95jd00690, 1995.
699 Mesinger, F., DiMego, G., Kalnay, E., Mitchell, K., Shafran, P. C., Ebisuzaki, W., Jovic,
700 D., Woollen, J., Rogers, E., Berbery, E. H., Ek, M. B., Fan, Y., Grumbine, R.,
701 Higgins, W., Li, H., Lin, Y., Manikin, G., Parrish, D., and Shi, W.: North
702 American regional reanalysis, B Am Meteorol Soc, 87, 343-360, 10.1175/Bams-
703 87-3-343, 2006.
704 Miyasaka, T., and Nakamura, H.: Structure and formation mechanisms of the northern
705 hemisphere summertime subtropical highs, J Climate, 18, 5046-5065, Doi
706 10.1175/Jcli3599.1, 2005.

Morman, S. A., and Plumlee, G. S.: The role of airborne mineral dusts in human disease, Aeolian Res, 9, 203-212, 10.1016/j.aeolia.2012.12.001, 2013.

Myoung, B., and Nielsen-Gammon, J. W.: Sensitivity of Monthly Convective Precipitation to Environmental Conditions, J Climate, 23, 166-188, 10.1175/2009jcli2792.1, 2010a.

Myoung, B., and Nielsen-Gammon, J. W.: The Convective Instability Pathway to Warm Season Drought in Texas. Part I: The Role of Convective Inhibition and Its Modulation by Soil Moisture, J Climate, 23, 4461-4473, 10.1175/2010jcli2946.1, 2010b.

O'Brien, R. M.: A caution regarding rules of thumb for variance inflation factors, Qual Quant, 41, 673-690, 10.1007/s11135-006-9018-6, 2007.

Perry, K. D., Cahill, T. A., Eldred, R. A., Dutcher, D. D., and Gill, T. E.: Long-range transport of North African dust to the eastern United States, J Geophys Res-Atmos, 102, 11225-11238, Doi 10.1029/97jd00260, 1997.

Prein, A. F., Holland, G. J., Rasmussen, R. M., Clark, M. P., and Tye, M. R.: Running dry: The US Southwest's drift into a drier climate state, Geophys Res Lett, 43, 1272-1279, 10.1002/2015gl066727, 2016.

Prospero, J. M.: Long-range transport of mineral dust in the global atmosphere: Impact of African dust on the environment of the southeastern United States, P Natl Acad Sci USA, 96, 3396-3403, DOI 10.1073/pnas.96.7.3396, 1999a.

Prospero, J. M.: Long-term measurements of the transport of African mineral dust to the southeastern United States: Implications for regional air quality, J Geophys Res-Atmos, 104, 15917-15927, Doi 10.1029/1999jd900072, 1999b.

730 Prospero, J. M., Landing, W. M., and Schulz, M.: African dust deposition to Florida:
731 Temporal and spatial variability and comparisons to models, J Geophys Res-
732 Atmos, 115, 10.1029/2009jd012773, 2010.
733 Prospero, J. M., Collard, F. X., Molinie, J., and Jeannot, A.: Characterizing the annual
734 cycle of African dust transport to the Caribbean Basin and South America and its
735 impact on the environment and air quality, Global Biogeochem Cy, 28, 757-773,
736 10.1002/2013gb004802, 2014.
737 Pu, B., and Dickinson, R. E.: Diurnal Spatial Variability of Great Plains Summer
738 Precipitation Related to the Dynamics of the Low-Level Jet, J Atmos Sci, 71,
739 1807-1817, 10.1175/Jas-D-13-0243.1, 2014.
740 Pu, B., Dickinson, R. E., and Fu, R.: Dynamical connection between Great Plains low-
741 level winds and variability of central Gulf States precipitation, J Geophys Res-
742 Atmos, 121, 3421-3434, 10.1002/2015jd024045, 2016a.
743 Pu, B., Fu, R., Dickinson, R. E., and Fernando, D. N.: Why do summer droughts in the
744 Southern Great Plains occur in some La Nina years but not others?, J Geophys
745 Res-Atmos, 121, 1120-1137, 10.1002/2015jd023508, 2016b.
746 Pu, B., and Ginoux, P.: Projection of American dustiness in the late 21st century due to
747 climate change, Scientific Reports, 7:5553, 1-10, 10.1038/s41598-017-05431-9,
748 2017.
749 Riemann-Campe, K., Fraedrich, K., and Lunkeit, F.: Global climatology of Convective
750 Available Potential Energy (CAPE) and Convective Inhibition (CIN) in ERA-40
751 reanalysis, Atmos Res, 93, 534-545, 10.1016/j.atmosres.2008.09.037, 2009.

752 Ruane, A. C.: NARR's Atmospheric Water Cycle Components. Part I: 20-Year Mean and
753 Annual Interactions, J Hydrometeorol, 11, 1205-1219, 10.1175/2010jhm1193.1,
754 2010a.
755 Ruane, A. C.: NARR's Atmospheric Water Cycle Components. Part II: Summertime
756 Mean and Diurnal Interactions, J Hydrometeorol, 11, 1220-1233,
757 10.1175/2010jhm1279.1, 2010b.
758 Ruiz-Barradas, A., and Nigam, S.: Great plains hydroclimate variability: The view from
759 North American regional reanalysis, J Climate, 19, 3004-3010, Doi
760 10.1175/Jcli3768.1, 2006.
761 Sassen, K.: The Polarization Lidar Technique for Cloud Research - a Review and Current
762 Assessment, B Am Meteorol Soc, 72, 1848-1866, Doi 10.1175/1520-
763 0477(1991)072<1848:Tpltfc>2.0.Co;2, 1991.
764 Seager, R., Ting, M. F., Held, I., Kushnir, Y., Lu, J., Vecchi, G., Huang, H. P., Harnik,
765 N., Leetmaa, A., Lau, N. C., Li, C. H., Velez, J., and Naik, N.: Model projections
766 of an imminent transition to a more arid climate in southwestern North America,
767 Science, 316, 1181-1184, 10.1126/science.1139601, 2007.
768 Sorooshian, A., Wonaschutz, A., Jarjour, E. G., Hashimoto, B. I., Schichtel, B. A., and
769 Betterton, E. A.: An aerosol climatology for a rapidly growing arid region
770 (southern Arizona): Major aerosol species and remotely sensed aerosol properties,
771 J Geophys Res-Atmos, 116, 10.1029/2011jd016197, 2011.
772 Tong, D. Q., Wang, J. X. L., Gill, T. E., Lei, H., and Wang, B. Y.: Intensified dust storm
773 activity and Valley fever infection in the southwestern United States, Geophys
774 Res Lett, 44, 4304-4312, 10.1002/2017gl073524, 2017.

775 Weaver, S. J., and Nigam, S.: Variability of the great plains low-level jet: Large-scale
776 circulation context and hydroclimate impacts, J Climate, 21, 1532-1551,
777 10.1175/2007jcli1586.1, 2008.
778 Winker, D. M., Hunt, W., and Hostetler, C.: Status and performance of the CALIOP
779 lidar, Bba Lib, 5575, 8-15, 10.1117/12.571955, 2004.
780 Winker, D. M., Hunt, W. H., and McGill, M. J.: Initial performance assessment of
781 CALIOP, Geophys Res Lett, 34, 10.1029/2007gl030135, 2007.
782 Wu, G. X., and Liu, Y. M.: Summertime quadruplet heating pattern in the subtropics and
783 the associated atmospheric circulation, Geophys Res Lett, 30,
784 10.1029/2002gl016209, 2003.
785 Ye, B., Del Genio, A. D., and Lo, K. K. W.: CAPE variations in the current climate and
786 in a climate change, J Climate, 11, 1997-2015, Doi 10.1175/1520-0442-
787 11.8.1997, 1998.
788 Yu, H. B., Remer, L. A., Chin, M., Bian, H. S., Tan, Q., Yuan, T. L., and Zhang, Y.:
789 Aerosols from Overseas Rival Domestic Emissions over North America, Science,
790 337, 566-569, 10.1126/science.1217576, 2012.
791 Zender, C. S., Bian, H. S., and Newman, D.: Mineral Dust Entrainment and Deposition
792 (DEAD) model: Description and 1990s dust climatology, J Geophys Res-Atmos,
793 108, 10.1029/2002jd002775, 2003.
794 Zhang, L., Henze, D. K., Grell, G. A., Torres, O., Jethva, H., and Lamsal, L. N.: What
795 factors control the trend of increasing AAOD over the United States in the last
796 decade?, J. Geophys. Res. Atmos, 122, 1797-1810, 10.1002/2016JD025472,
797 2017.
798

Table 1 Correlations between friction velocity (U^*) and CIN, CIN and 2 meter temperature (T_{2m}), T_{2m} and U^*, T_{700}-T_{dp} (the differences between air temperature at 700 hPa and 2m dew point temperature) and CIN, T_{700}-T_{dp} and U^* for all days in JJA from 2002 to 2015 (1288 days), days when fine dust concentration is available (431 days), and dusty days (52 days). All values are significant at the 95% confidence level (t-test) except those listed in italic.

Table 2 Correlations between U^* and CIN, CIN and vertical wind speed at 850 hPa (w850), w850 and U^* during dusty days in JJA from 2002 to 2015. All values are significant at the 95% confidence level except the value significant at the 90% confidence level is labeled with a "+" (t-test).

822 Figure 1. Trend (shading) of fine dust concentration (μg m^{-3}) from 1990 to 2015 in (a)
823 DJF, (b) MAM, (c) JJA, and (d) SON from IMPROVE gridded data. Dotted areas are
824 significant at the 95% confidence level. The colored circles show the trend at IMPROVE
825 stations with consecutive records for at least 23 years during 1990-2015. Circles with
826 green outlines denote that the trend is significant at the 90% confidence level. Black
827 boxes denote the averaging areas of the southwestern U.S. (solid) and the Great Plains
828 (dashed).
829
830 Figure 2. (a)-(d) Multiple linear regression coefficients calculated by regressing fine dust
831 concentration from 1990-2015 onto standardized precipitation (purple), bareness
832 (orange), and surface wind (green). Color denotes the most influential factor at each grid
833 (i.e., the largest regression coefficient in absolute value among the three), while
834 saturation of the color shows the magnitude of the coefficient (0 to 0.3). Areas significant
835 at the 95% confidence levels are dotted. (e) Bar-plot showing the correlations between
836 observed regional mean fine dust concentration and the reconstructed concentration using
837 3, 4, and 5 controlling factors (light, median, and deep blue), and pattern correlation
838 between trends from the observation and from reconstructed fine dust using 3, 4, and 5
839 factors (light, medium, and deep pink) in the Great Plains (GP) and the southwestern U.S.
840 (WST, black boxes in a-d). "3-factor" denotes precipitation, bareness, and surface wind,
841 "4-factor" denotes precipitation, bareness, surface wind, and CIN, "5-factor" denotes
842 precipitation, bareness, surface wind, CIN, and CAPE. Black boxes denote the averaging
843 areas of the WST (solid) and GP (dashed).
844

Figure 3. (a) Observed (Obs) and reconstructed (Reg) trends of fine dust concentration (μg m^{-3}) using three factors in spring from 1990 to 2015. The contributions from each factor (precipitation, bareness, and surface wind) to the overall reconstructed trend are also shown (second row). Dotted areas are significant at the 90% confidence level. Pattern correlation between reconstructed dust concentration trends and observed trends in the domain (25°-49.5°N, 66.5°-125°W) are shown at the top right corner of each plot. Black box denotes the southwestern U.S. (WST). (b) Time series of fine dust concentration (cyan) and precipitation (purple) averaged over the WST and their linear trends (dashed lines; values are listed at bottom left) in spring from 1990 to 2015. Gray shading denotes ±one standard error of the observations. The correlation between fine dust and precipitation is also listed at the bottom in purple.

Figure 4. (a) Observed (Obs) and reconstructed (Reg) tends of fine dust concentration (μg m^{-3}) using five factors in summer from 1990-2015. The contributions from each factor (precipitation, bareness, surface wind, CAPE, and CIN) are also shown (second and third rows). Dotted areas are significant at the 90% confidence level. Pattern correlation between reconstructed dust concentration trends and the observed trends in the domain (25°-49.5°N, 66.5°-125°W) are shown at the right corner of each plot. Black box denotes the central Great Plains (CGP). (b) Time series of fine dust concentration (cyan), CIN (orange), and CAPE (deep blue) averaged over the CGP and their linear trends (dashed lines) in summer from 1990-2015. Gray shading denotes ±one standard error of the observations. (c) Time series of T_{700}-T_{dp} (black), T_{700} (green) and T_{dp} (light blue) and their linear trends (dashed lines) in summer from 1990 to 2015.

868 Figure 5. (a) Time series of fine dust concentration (μg m^{-3}) averaged in the CGP (cyan)
869 and the index of the Great Plains low-level jet (magenta) and their trends (dashed line) in
870 JJA from 1990 to 2015. Gray shading denotes ±one standard error of the observations.
871 Correlations between the jet index and fine dust concentration, CIN, and near surface
872 wind speed for (b) 1990-2015 and (c) 2002-2015. Colored circles denotes correlations at
873 IMPROVE stations, with green outlines denotes the correlation is significant at the 90%
874 confidence level. Areas significant at the 95% confidence level are dotted in (b) and
875 significant at the 90% confidence level are dotted in (c). Black box in (b)-(c) denotes the
876 CGP region, and deep pink box denotes the averaging area for the jet index.
877 Figure 6. Scatter plot of standardized friction velocity (U^*) and CIN anomalies for (a) all
878 days in JJA from 2002-2015, (b) days when fine dust data are available, and (c) dusty
879 days (when daily fine dust concentration anomaly is greater than one standard deviation).
880
881 Figure 7. Nighttime 532 nm total attenuated backscatter (shading) and depolarization
882 ratio (black contours, values ≥ 0.2 are shown) from CALIOP on August 10th, 2007 (top
883 left) and on June 21st, 2013 (bottom left), along with daily anomalies of fine dust
884 concentration (μg m^{-3}; shading, right column) and CIN (blue contour, only negative
885 values from -60 to -120 J kg^{-1} are shown). CALIOP orbit tracks are shown in grey lines
886 (right column) with cyan part and sampling points (A-F) denote the cross-section shown
887 on the left column. Black boxes denote the CGP region.
888
889 Figure 8. Same as Fig. 7 but for July 2nd, 2011 (top) and July 2nd, 2012 (bottom). Only
890 positive CIN anomalies from 25 to 50 J kg^{-1} are shown (light purple contour).

Figure 9. Daily composites of the anomalies of (a) fine dust concentration (μg m^{-3}), (b) CIN (J kg^{-1}), (c) CAPE (J kg^{-1}), (d) 900 hPa wind speed (m s^{-1}), (e) 10 m wind speed (m s^{-1}), (f) U^* (m s^{-1}), (g) total precipitation (mm day^{-1}), (h) convective precipitation (mm day^{-1}), and (i) total cloud cover (%) during dusty days in JJA from 2002 to 2015. Dotted areas are significant at the 95% confidence level. 900 hPa and 10 m wind anomalies (green vectors) significant at the 95% confidence level are shown in (d) and (e), respectively. Black boxes denote the CGP region.

Figure 10. Daily composite of the anomalies of vertical velocity (shading; 10^{-2} m s^{-1}), potential temperature (grey contours; K), and specific humidity (purple contours; g kg^{-1}) from the ERA-Interim, and fine dust concentration anomalies (bottom; orange line) averaged between 95° and 102° W for dusty days in JJA from 2002 to 2015. Dotted area denotes vertical velocity significant at the 90% confidence level. Topography is masked out in grey. Cyan lines denote the domain of the CGP.

Figure 11. Daily composites of the anomalies of (a) T_{2m} (K) and (b) 850 hPa geopotential height (gpm) and horizontal wind vectors (m s^{-1}; grey) from the ERA-Interim averaged over dusty days in JJA from 2002-2015. Blue and red contours in (b) denote 1560 gpm in the climatology (2002-2015) and during dusty days, respectively. Areas significant at the 95% confidence level are dotted. Wind vectors significant at the 95% confidence level are plotted in green. Black boxes denote the CGP region.

Table 1 Correlations between friction velocity (U^*) and CIN, CIN and 2 meter temperature (T_{2m}), T_{2m} and U^*, T_{700}-T_{dp} (the differences between air temperature at 700 hPa and 2m dew point temperature) and CIN, T_{700}-T_{dp} and U^* for all days in JJA from 2002 to 2015 (1288 days), days when fine dust concentration is available (431 days), and dusty days (52 days). All values are significant at the 95% confidence level (t-test) except those listed in italic.

Variables	**All days in JJA**	**Available days**	**Dusty days**
U^*, CIN	-0.54	-0.54	-0.44
CIN, T_{2m}	-0.59	-0.59	-0.39
T_{2m}, U^*	0.39	0.37	*0.19*
CIN, T_{700}-T_{dp}	-0.59	-0.62	-0.59
T_{700}-T_{dp}, U^*	0.37	0.38	*0.14*

Table 2 Correlations between U^* and CIN, CIN and vertical wind speed at 850 hPa (w850), w850 and U^* during dusty days in JJA from 2002 to 2015. All values are significant at the 95% confidence level except the value significant at the 90% confidence level is labeled with a "+" (t-test).

Variables	**Dusty days**
U^*, CIN	-0.44
CIN, w850	0.28^+
w850, U^*	-0.32

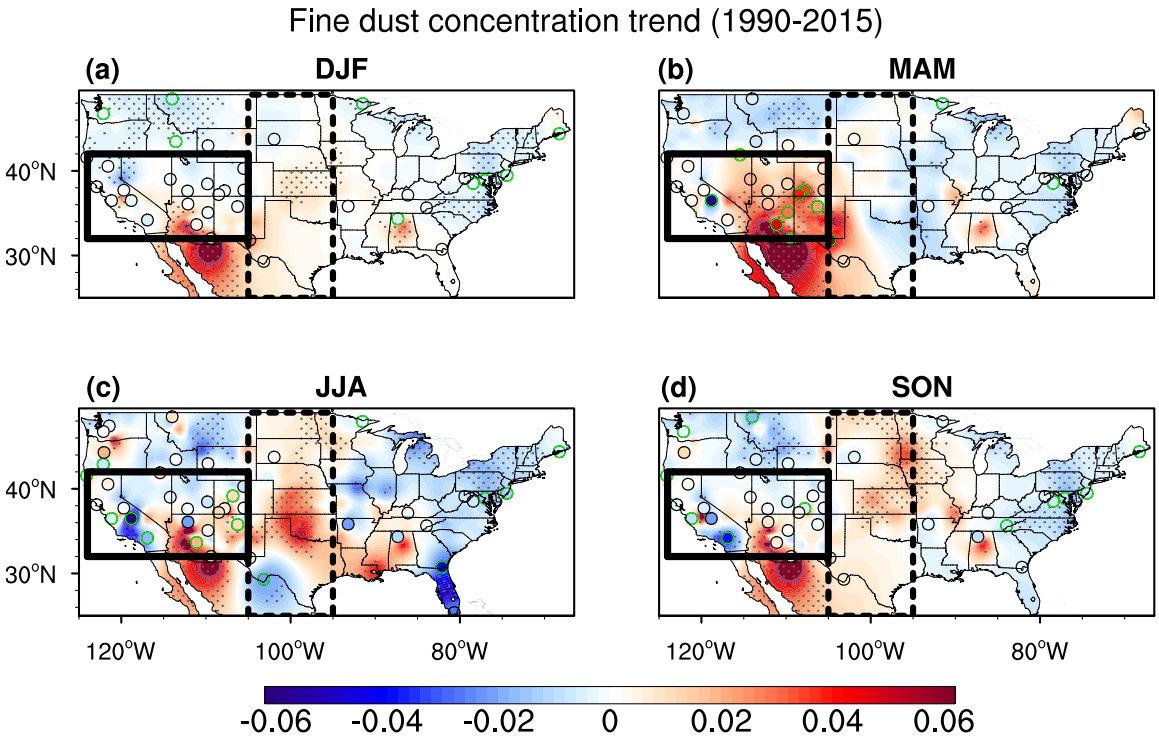

Figure 1. Trend (shading) of fine dust concentration (μg m^{-3}) from 1990 to 2015 in (a) DJF, (b) MAM, (c) JJA, and (d) SON from IMPROVE gridded data. Dotted areas are significant at the 95% confidence level. The colored circles show the trend at IMPROVE stations with consecutive records for at least 23 years during 1990-2015. Circles with green outlines denote that the trend is significant at the 90% confidence level. Black boxes denote the averaging areas of the southwestern U.S. (solid) and the Great Plains (dashed).

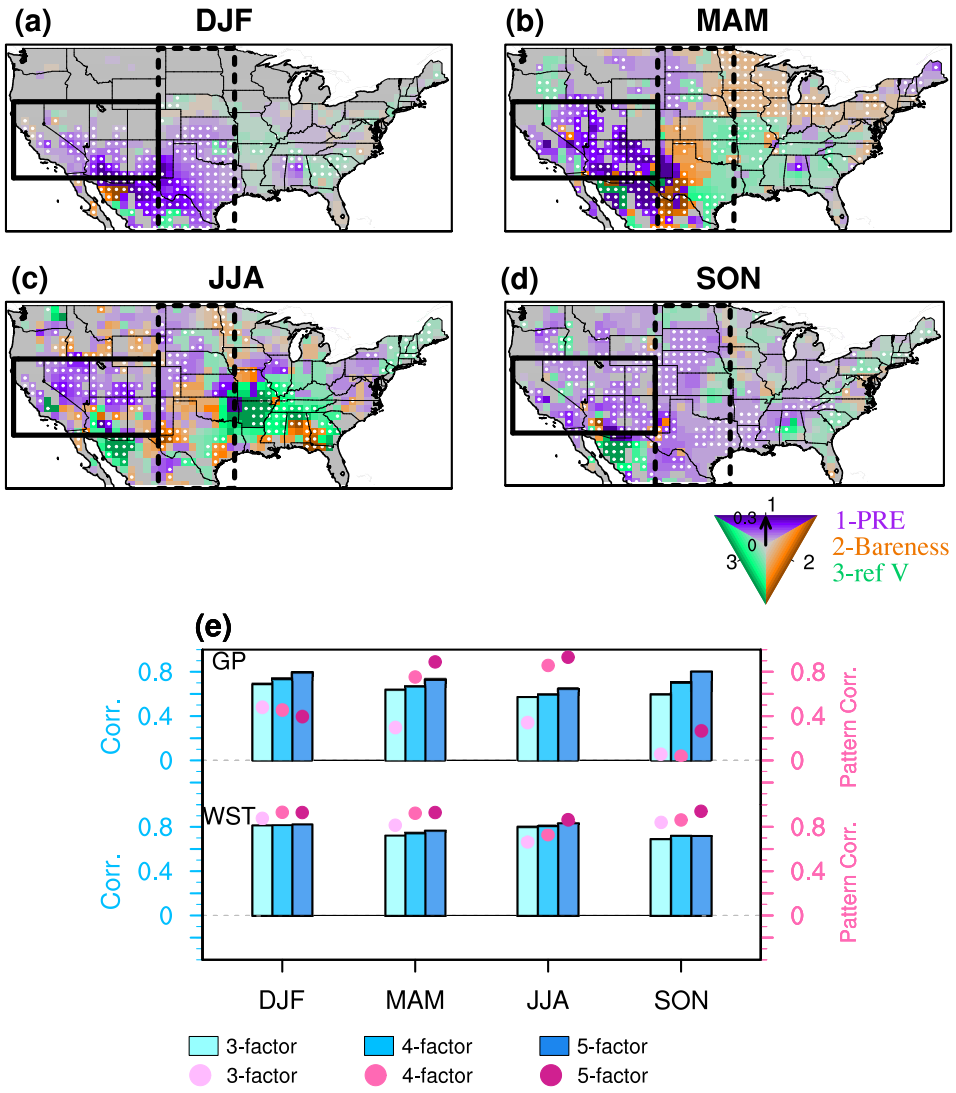

Figure 2. (a)-(d) Multiple linear regression coefficients calculated by regressing fine dust concentration from 1990-2015 onto standardized precipitation (purple), bareness (orange), and surface wind (green). Color denotes the most influential factor at each grid (i.e., the largest regression coefficient in absolute value among the three), while saturation of the color shows the magnitude of the coefficient (0 to 0.3). Areas significant at the 95% confidence levels are dotted. (e) Bar-plot showing the correlations between observed regional mean fine dust concentration and the reconstructed concentration using 3, 4, and 5 controlling factors (light, median, and deep blue), and pattern correlation between trends from the observation and from reconstructed fine dust using 3, 4, and 5 factors (light, medium, and deep pink) in the Great Plains (GP) and the southwestern U.S. (WST, black boxes in a-d). "3-factor" denotes precipitation, bareness, and surface wind, "4-factor" denotes precipitation, bareness, surface wind, and CIN, "5-factor" denotes precipitation, bareness, surface wind, CIN, and CAPE. Black boxes denote the averaging areas of the WST (solid) and GP (dashed).

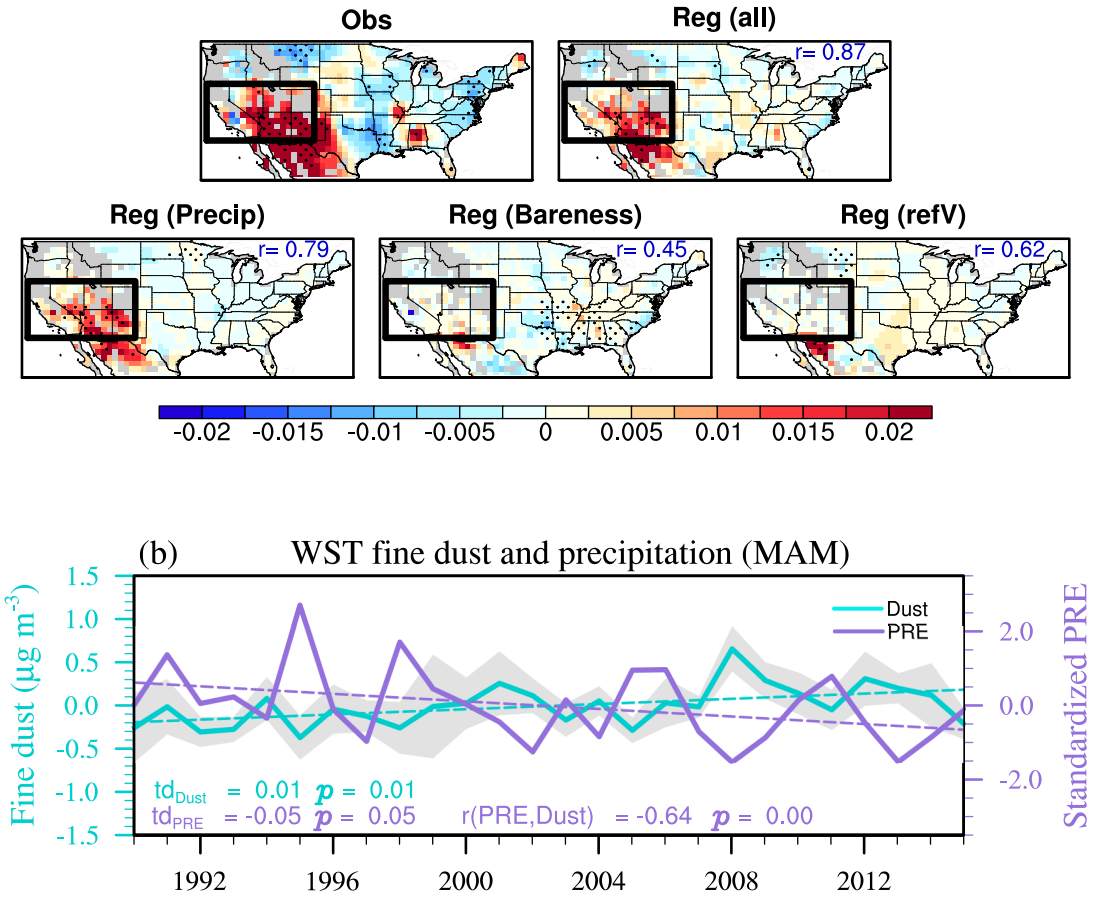

Figure 3. (a) Observed (Obs) and reconstructed (Reg) trends of fine dust concentration (μg m^{-3}) using three factors in spring from 1990 to 2015. The contributions from each factor (precipitation, bareness, and surface wind) to the overall reconstructed trend are also shown (second row). Dotted areas are significant at the 90% confidence level. Pattern correlation between reconstructed dust concentration trends and observed trends in the domain (25°-49.5°N, 66.5°-125°W) are shown at the top right corner of each plot. Black box denotes the southwestern U.S. (WST). (b) Time series of fine dust concentration (cyan) and precipitation (purple) averaged over the WST and their linear trends (dashed lines; values are listed at bottom left) in spring from 1990 to 2015. Gray shading denotes ±one standard error of the observations. The correlation between fine dust and precipitation is also listed at the bottom in purple.

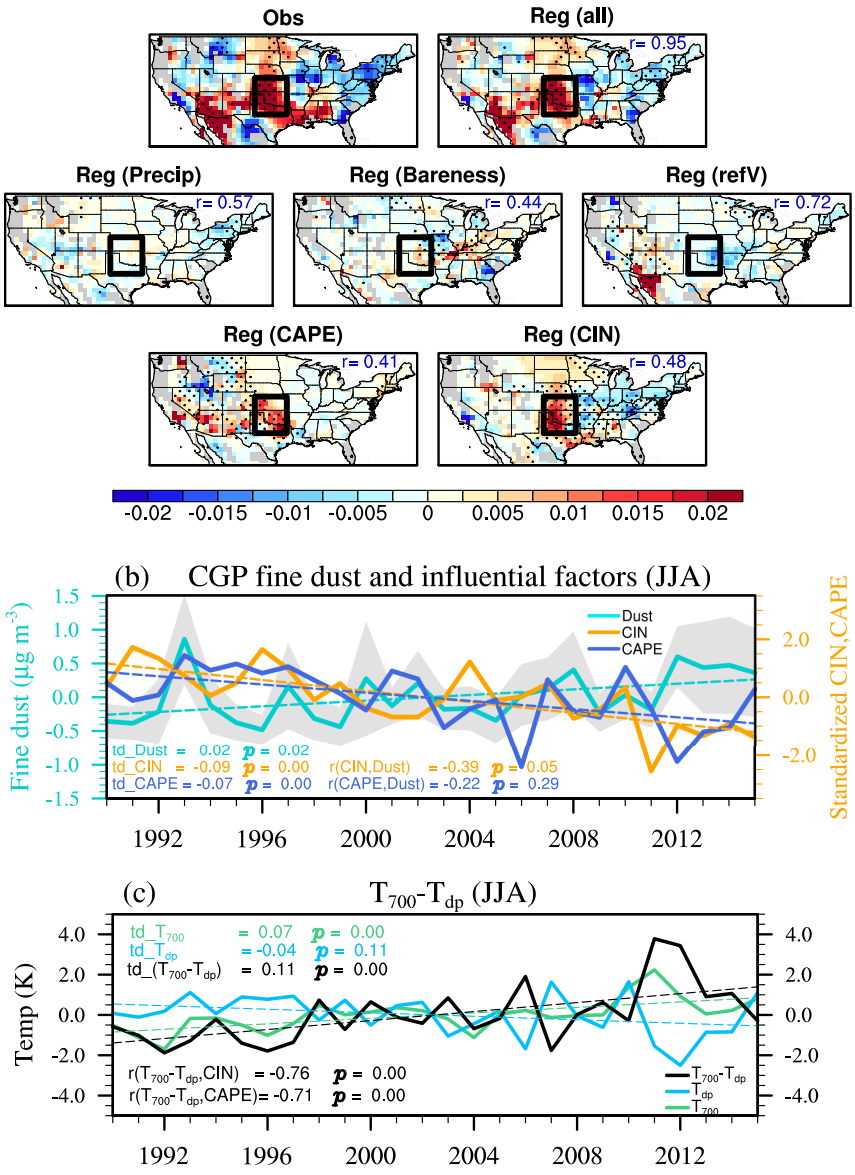

Figure 4. (a) Observed (Obs) and reconstructed (Reg) tends of fine dust concentration (μg m^{-3}) using five controlling factors in summer from 1990-2015. The contributions from each factor (precipitation, bareness, surface wind, CAPE, and CIN) are also shown (second and third rows). Dotted areas are significant at the 90% confidence level. Pattern correlation between reconstructed dust concentration trends and the observed trends in the domain (25°-49.5°N, 66.5°-125°W) are shown at the right corner of each plot. Black box denotes the central Great Plains (CGP). (b) Time series of fine dust concentration (cyan), CIN (orange), and CAPE (deep blue) averaged over the CGP and their linear trends (dashed lines) in summer from 1990-2015. Gray shading denotes ±one standard error of the observations. (c) Time series of T_{700}-T_{dp} (black), T_{700} (green) and T_{dp} (light blue) and their linear trends (dashed lines) in summer from 1990 to 2015.

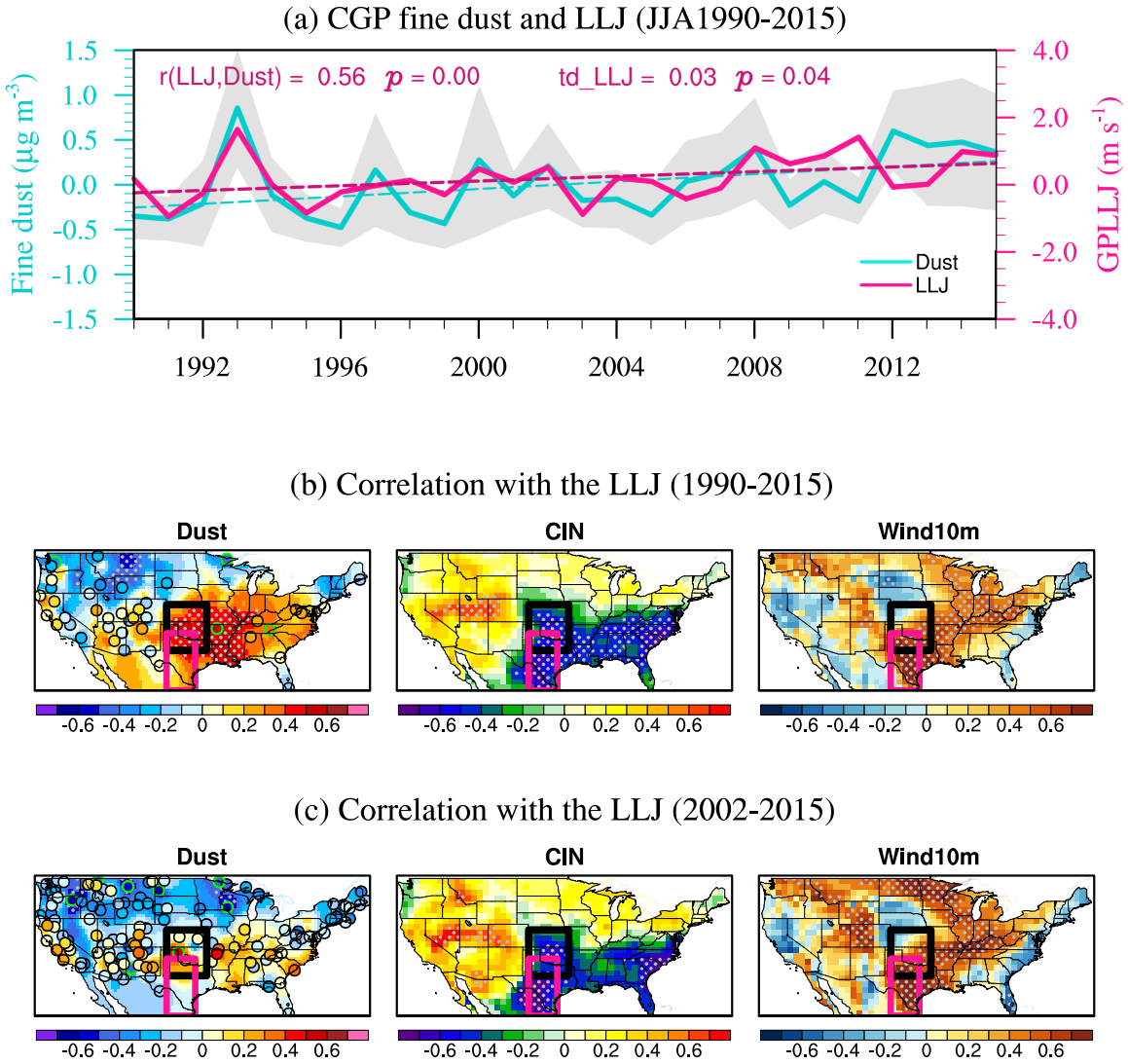

Figure 5. (a) Time series of fine dust concentration (μg m^{-3}) averaged in the CGP (cyan) and the index of the Great Plains low-level jet (magenta) and their trends (dashed line) in JJA from 1990 to 2015. Gray shading denotes ±one standard error of the observations. Correlations between the jet index and fine dust concentration, CIN, and near surface wind speed for (b) 1990-2015 and (c) 2002-2015. Colored circles denotes correlations at IMPROVE stations, with green outlines denotes the correlation is significant at the 90% confidence level. Areas significant at the 95% confidence level are dotted in (b) and significant at the 90% confidence level are dotted in (c). Black box in (b)-(c) denotes the CGP region, and deep pink box denotes the averaging area for the jet index.

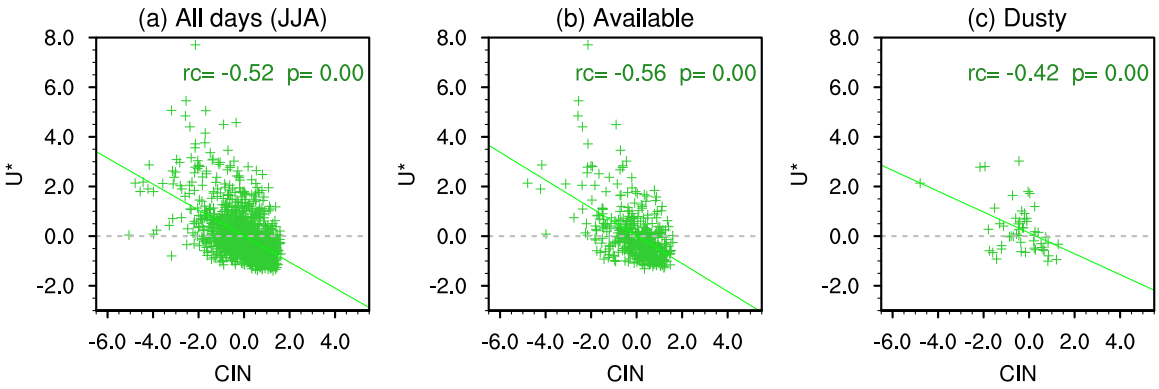

Figure 6. Scatter plot of standardized friction velocity (U^*) and CIN anomalies for (a) all days in JJA from 2002-2015, (b) days when fine dust data are available, and (c) dusty days (when daily fine dust concentration anomaly is greater than one standard deviation).

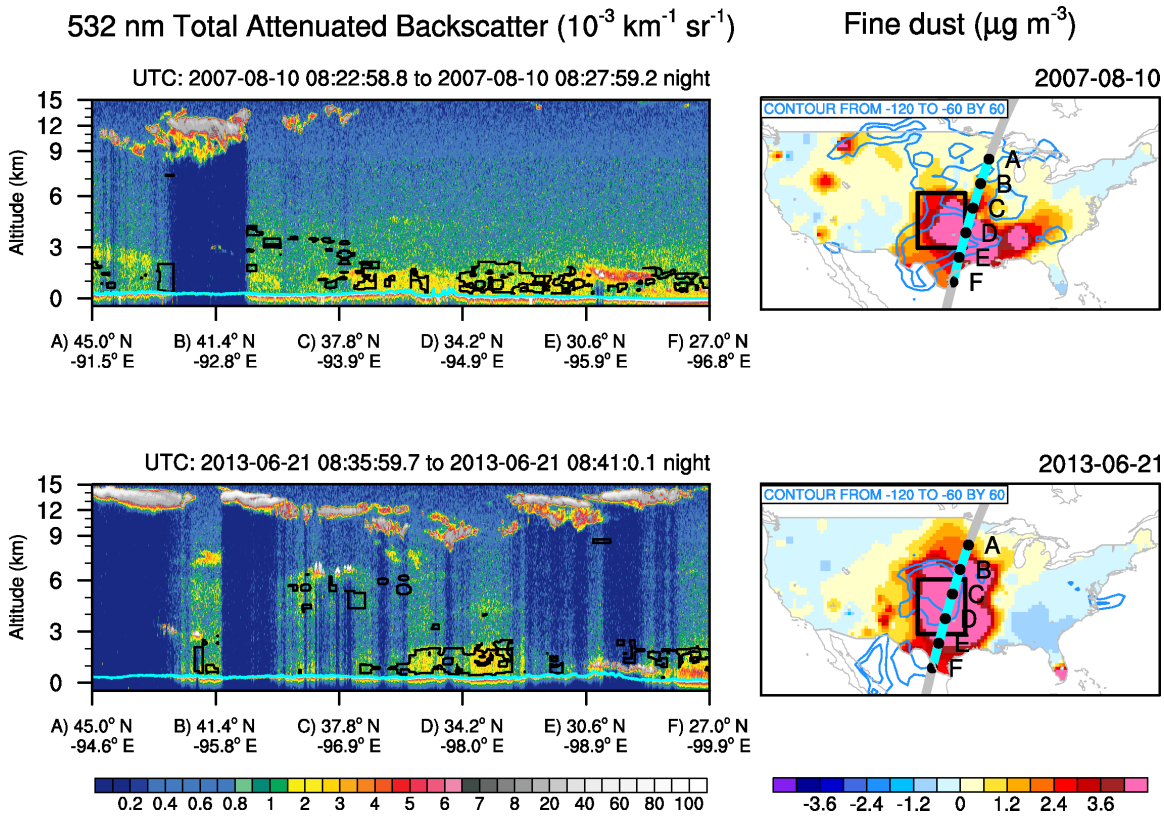

Figure 7. Nighttime 532 nm total attenuated backscatter (shading) and depolarization ratio (black contours, values ≥ 0.2 are shown) from CALIOP on August 10th, 2007 (top left) and on June 21st, 2013 (bottom left), along with daily anomalies of fine dust concentration (μg m^{-3}; shading, right column) and CIN (blue contour, only negative values from -60 to -120 J kg^{-1} are shown). CALIOP orbit tracks are shown in grey lines (right column) with cyan part and sampling points (A-F) denote the cross-section shown on the left column. Black boxes denote the CGP region.

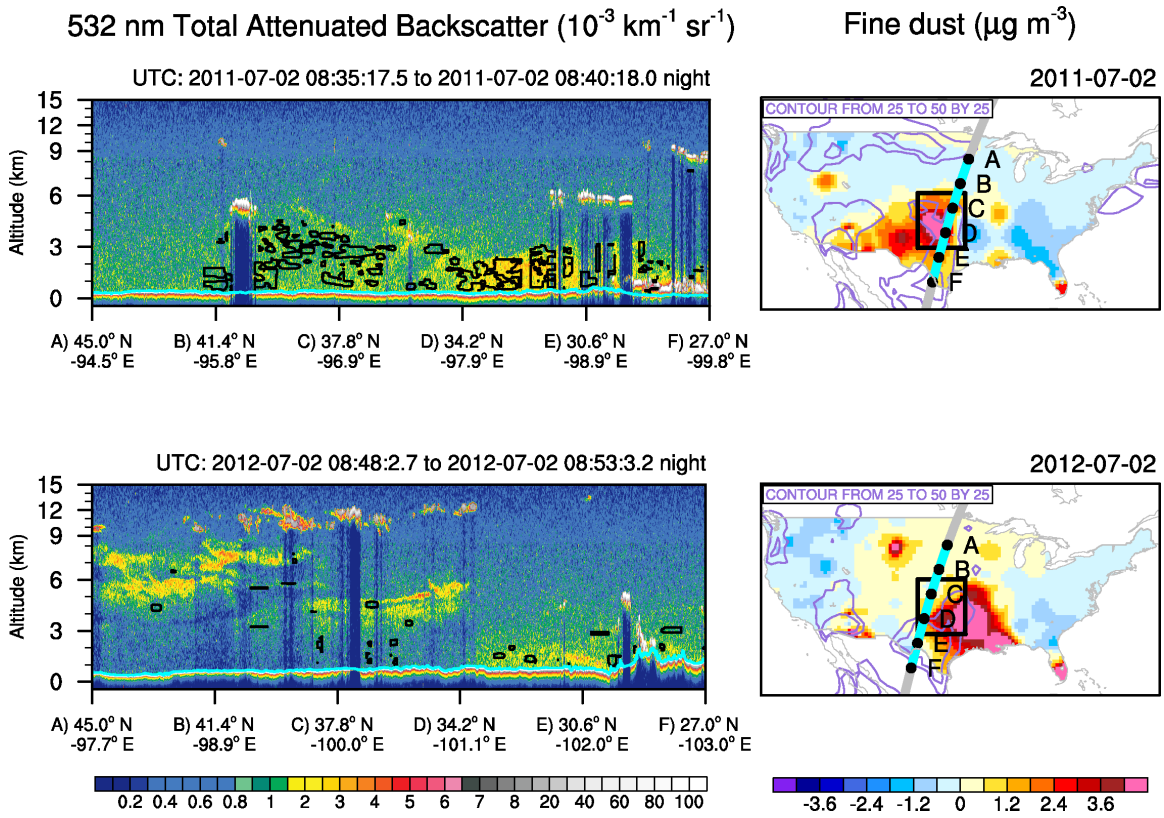

Figure 8. Same as Fig. 7 but for July 2nd, 2011 (top) and July 2nd, 2012 (bottom). Only positive CIN anomalies from 25 to 50 J kg^{-1} are shown (light purple contour).

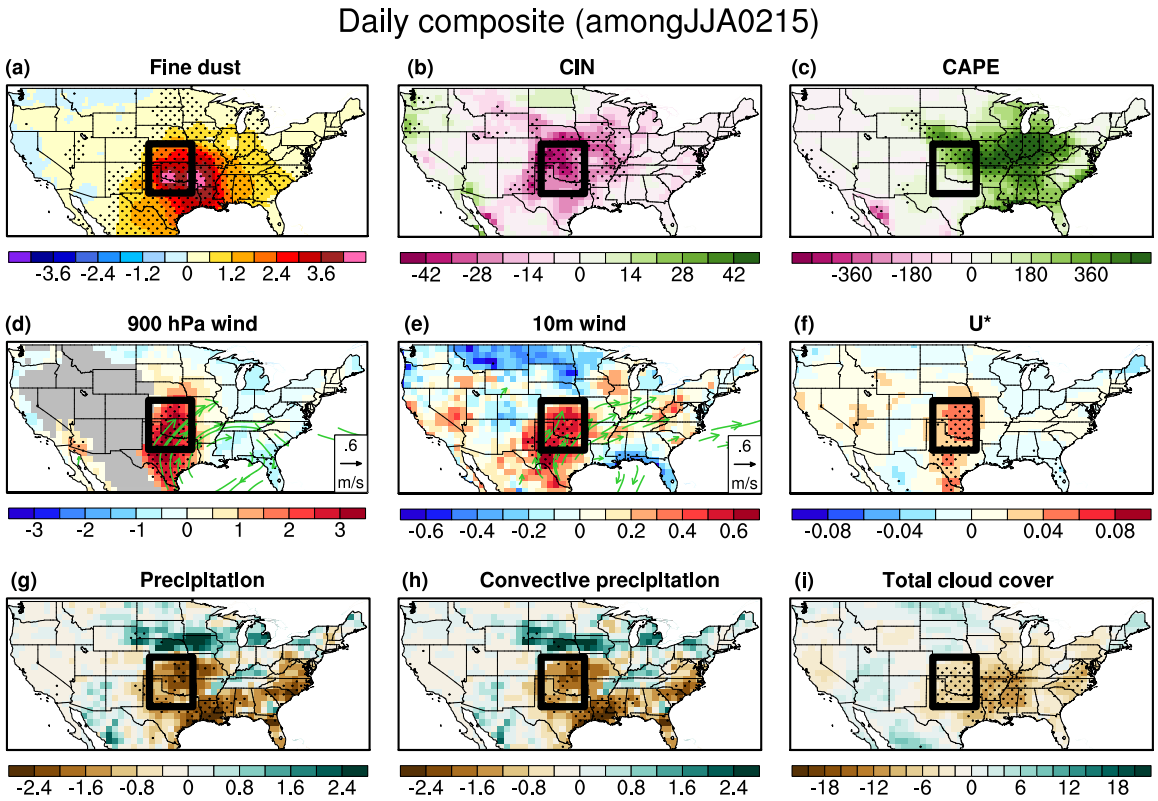

Figure 9. Daily composites of the anomalies of (a) fine dust concentration (μg m^{-3}), (b) CIN (J kg^{-1}), (c) CAPE (J kg^{-1}), (d) 900 hPa wind speed (m s^{-1}), (e) 10 m wind speed (m s^{-1}), (f) U^* (m s^{-1}), (g) total precipitation (mm day^{-1}), (h) convective precipitation (mm day^{-1}), and (i) total cloud cover (%) during dusty days in JJA from 2002 to 2015. Dotted areas are significant at the 95% confidence level. 900 hPa and 10 m wind anomalies (green vectors) significant at the 95% confidence level are shown in (d) and (e), respectively. Black boxes denote the CGP region.

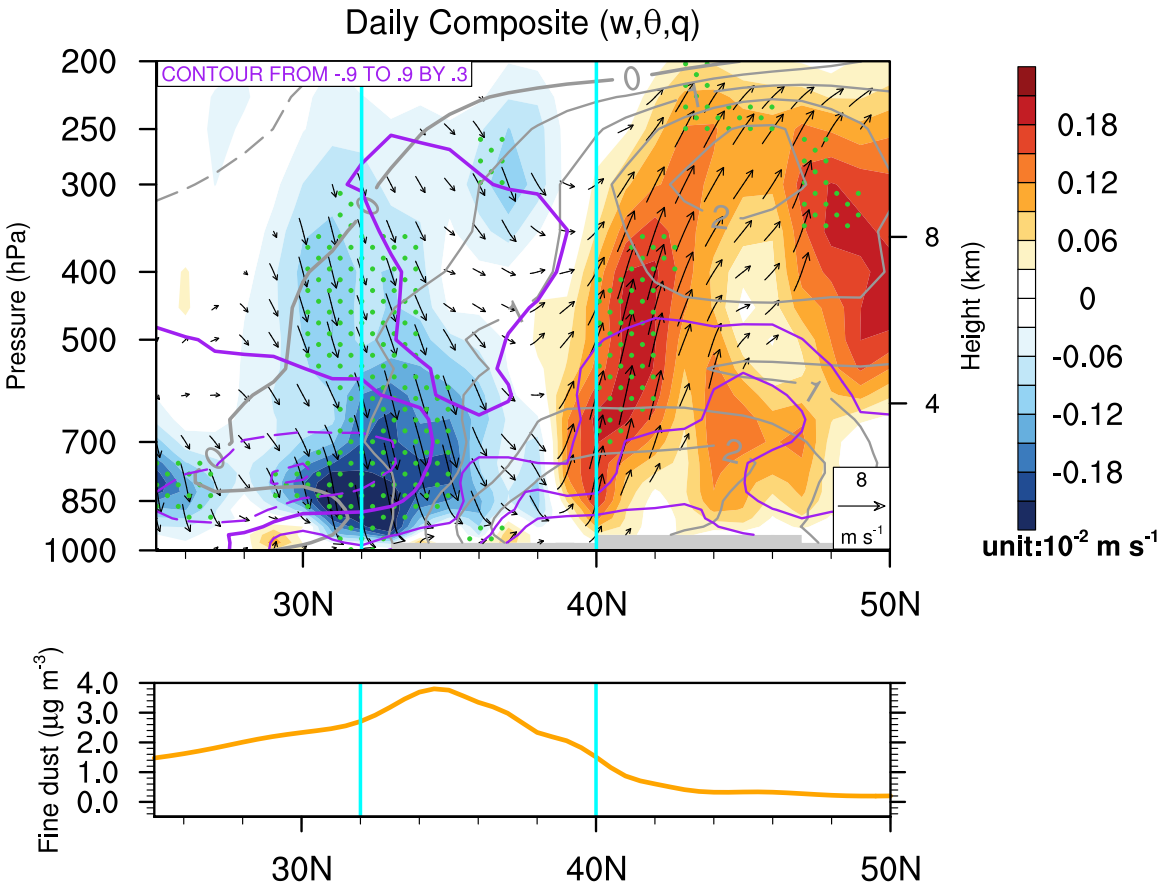

Figure 10. Daily composite of the anomalies of vertical velocity (shading; 10^{-2} m s^{-1}), potential temperature (grey contours; K), and specific humidity (purple contours; g kg^{-1}) from the ERA-Interim, and fine dust concentration anomalies (bottom; orange line) averaged between 95° and 102° W for dusty days in JJA from 2002 to 2015. Dotted area denotes vertical velocity significant at the 90% confidence level. Topography is masked out in grey. Cyan lines denote the domain of the CGP.

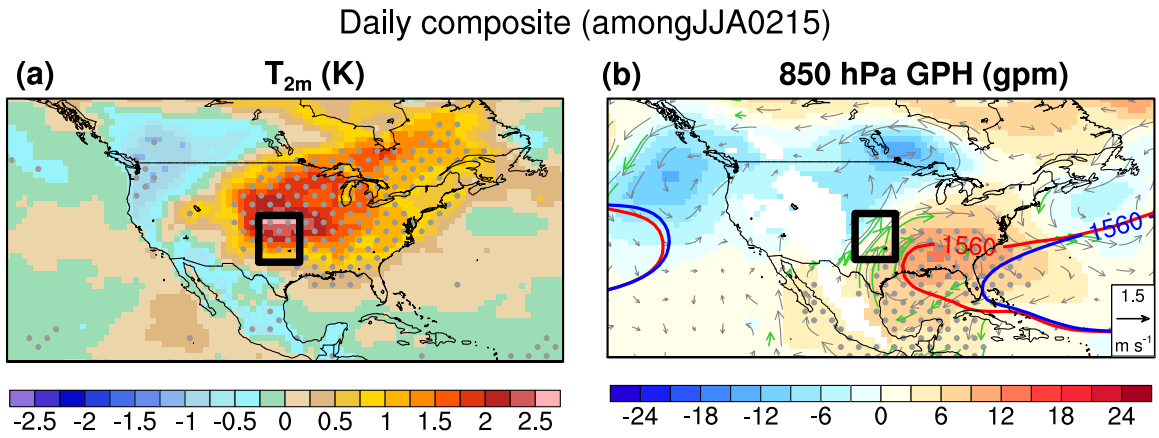

Figure 11. Daily composites of the anomalies of (a) T_{2m} (K) and (b) 850 hPa geopotential height (gpm) and horizontal wind vectors (m s^{-1}; grey) from the ERA-Interim averaged over dusty days in JJA from 2002-2015. Blue and red contours in (b) denote 1560 gpm in the climatology (2002-2015) and during dusty days, respectively. Areas significant at the 95% confidence level are dotted. Wind vectors significant at the 95% confidence level are plotted in green. Black boxes denote the CGP region.